JOURNAL OF GEOPHYSICAL RESEARCH, VOL. 98, NO. B5, PAGES 8107–8125, MAY 10, 1993

Determination of Source Parameters at Regional Distances With Three-Component Sparse Network Data

DOUGLAS S. DREGER

Seismographic Station, University of California, Berkeley

DONALD V. HELMBERGER

Seismological Laboratory, California Institute of Technology, Pasadena

We find remarkable similarities between regional body waves recorded by the TERRAscope network of broadband stations and synthetics constructed from a standard southern California velocity model. This model is shown to be effective for a variety of azimuths and ranges throughout southern California. At short periods some of the relative timing of the body waves are discordant, but at longer periods this becomes less of a factor. Thus we have developed a waveform inversion technique to rapidly determine source parameters using stored Green's functions for events out to 500 km, well outside the TERRAscope network. Often, only the three-component records of a single station are required because the ratio of SV to SH energy is dependent upon source orientation. Sensitivity analyses examining the effects of source mislocations and velocity model on the inversion results show that the long-period body waves appear relatively insensitive to lateral mislocations but are sensitive to source depth. However, the choice of velocity model can be a factor in obtaining reliable estimates of source depth. In this study the October 24, 1990, (M_w = 5.2) Lee Vining and the December 3, 1991, (M_w = 5.1) Baja California events are used to demonstrate the effectiveness of the inversion method. For the Baja event, we obtained unique results using a single station. For the Lee Vining event, inversions using a single station were not as stable. However, we found that using two stations with only a 24° aperture provided enough constraint to obtain unique results.

INTRODUCTION

The regional networks of broadband instrumentation currently being installed are expected to improve our understanding of wave propagation and source problems. Progress has been made in studying wave propagation at regional distances using the broadband, whole waveform data [*Helmberger et al.*, 1992*a*,*b*; *Zhao and Helmberger*, 1991]. These studies are providing information about both the P wave and S wave velocity structures. At local distances the study of wave propagation is further complicated by the greater influence of near-surface lateral heterogeneity and the small time separations between direct, reflected, converted, and surface wave phases; however, it seems possible to model the data broadband with simple, regionalized upper crustal models [*Dreger and Helmberger*, 1990].

The broadband characteristics of the high-quality data are especially useful because they allow the selection of the bandwidth which is the most sensitive to the problem at hand. Long-period data have traditionally been found to be particularly useful in source problems. There are numerous examples of the use of teleseismic body waves to obtain estimates of source parameters of large earthquakes ($m_b \geq 6.0$) in the literature. Smaller events, however, are recorded with poor signal-to-noise ratios at distances greater than 30°. This is especially true for strike-slip earthquakes that have a P wave radiation node for diving energy. In addition, surface wave studies at teleseismic distances are also subject to poor signal-to-noise ratios for moderate sized earthquakes. To circumvent this problem, data recorded at regional distances ($1° - 12°$) are used. Although the regional waveforms are relatively more complicated, the long-period P_{nl} waves are relatively stable (i.e., change slowly with distance) [*Helmberger and Engen*, 1980] and have proven to be quite successful in source inversions [*Wallace et al.*, 1981]. PL waves propagating in the upper crust (along a shallow interface at approximately 4 to 6 km depth) also appear to be stable and are useful in obtaining source parameters of earthquakes in the near-regional distance range (100 km to 300 km) [*Dreger and Helmberger*, 1991*a*]. There is evidence that source depth can be resolved with the long-period data [*Dreger and Helmberger*, 1991*a*,*b*], but source time histories and other higher-order source processes such as directivity and/or distributed rupture require shorter-period information and an Earth structure that adequately explains the short-period propagation characteristics. The wide dynamic range of these systems allows studies of both small and large earthquakes in a given source region enabling the isolation of source and

Paper number 93JB00023.
0148-0227/93/93JB-00023$05.00

propagation terms. This property provides a great advantage over the older systems where observations of mainshock-aftershock data occurred only rarely, when low-gain and high-gain instruments were colocated [see *Helmberger et al.*, 1992*a*].

The regional broadband networks will provide excellent coverage for the larger events; however, for smaller earthquakes, coverage will not be as good due to reduced signal-to-noise ratios. For smaller events it is necessary to investigate the sources of earthquakes with techniques appropriate for sparse networks or single stations. This is especially important for the studies of earthquakes not located in regions of dense instrumentation and historic earthquakes. Some progress has already been made at the inversion of waveform data recorded at a single station at local distances (< 100 km) [*Dreger and Helmberger*, 1991*a*; *Fan and Wallace*, 1991]. The former utilized a methodology where the Green's functions were tuned for a specific source-receiver path allowing the inversion of the whole low-pass-filtered waveform for seismic moment and focal mechanism parameters. Directivity and slip complexity were investigated by using the short-period information and making comparisons between events spanning several orders of magnitude in size. The latter investigated the effects of crustal structure on a moment tensor inversion of broadband displacement records. They found that it is possible to determine source parameters with relatively simple models at local distances but that source depth determinations are strongly model dependent. In addition, it has been shown that adding the direct P and S amplitude data to constrain first-motion mechanism analyses is also effective at local distances [*Ma and Kanamori*, 1991].

The purpose of this paper is to describe a procedure of obtaining source parameters such as focal mechanism, seismic moment, and source depth from regional data with sparse coverage and demonstrate its usefulness with data from the TERRAscope network of broadband stations. In particular, we apply a method that has proven successful in modeling regional P_{nl} waves and extend it to include the whole three-component record, excluding surface waves. The effects of hypocentral mislocations are studied with synthetic test cases. The method is applied to two recent, moderate sized earthquakes whose energy traversed com-

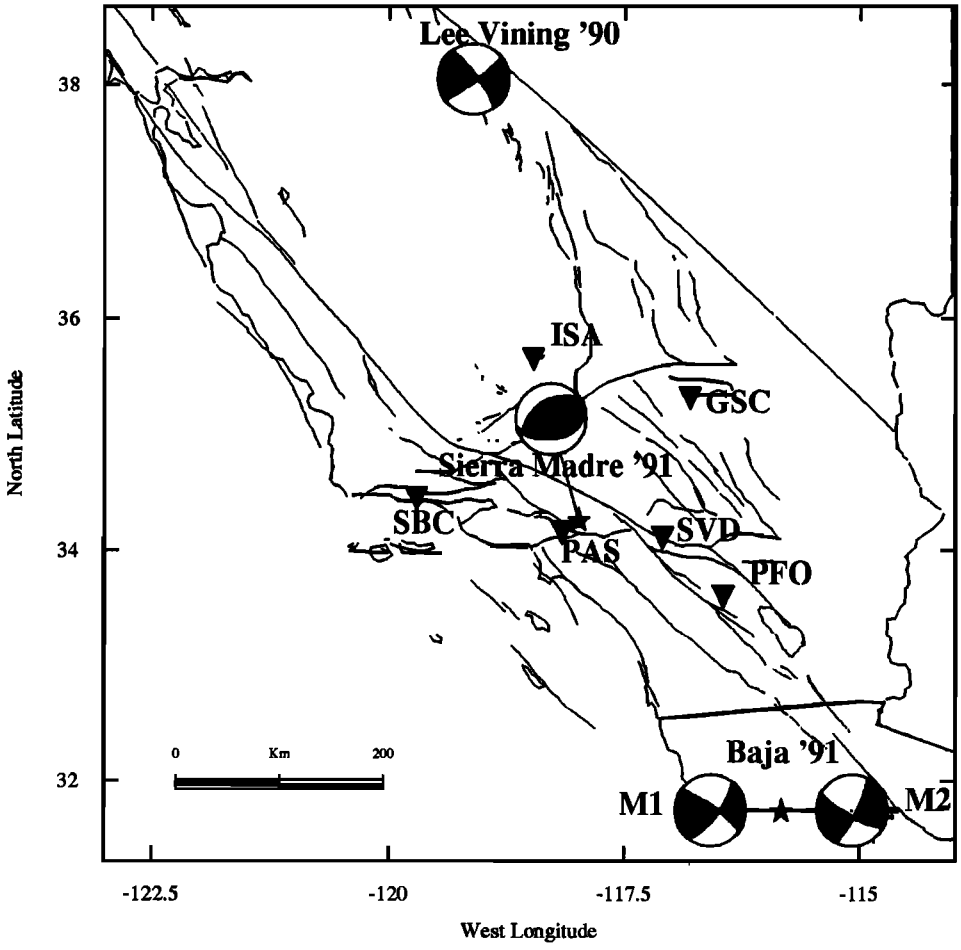

Fig. 1. Map showing the locations of the TERRAscope stations currently operational (inverted triangles) and the locations of the three events considered in this study. The mechanisms were determined by inversion of three-component data recorded by TERRAscope. M1 and M2 refer to mechanisms determined by inverting only data recorded at PAS (M1) and at both PAS and PFO (M2).

pletely different paths. We also examine the critical assumption that the velocity model is known. It does seem that although crustal structures are complex, adequate Green's functions may be calculated with relatively simple plane-layered velocity models derived independently from travel time studies as is demonstrated below.

A Case for the Standard Southern California Velocity Model

Although this study is primarily concerned with source retrieval from sparse network data it is interesting to consider first, a case in which there is good azimuthal coverage. Figure 1 shows the locations of the TERRAscope stations relative to the 1990 Lee Vining, 1991 Sierra Madre, and the 1991 Baja California earthquakes. The June 28, 1991, Sierra Madre earthquake ($M_L = 5.8$) was the topic of an earlier study in which the three-component, long-period body waves were inverted for source parameters [*Dreger and Helmberger*, 1991*a*]. The following section discusses the inversion method used in this and the earlier studies.

The Sierra Madre earthquake was optimally located within the TERRAscope network and was recorded by all six TERRAscope stations in operation at the time, with very good azimuthal coverage. Four of the stations were located at distances of 159 ± 1 km from the event. We inverted the long-period body wave data for that event and obtained results that were in excellent agreement with solutions obtained from first-motion polarities (E. Hauksson, The 1991 Sierra Madre earthquake sequence in southern California: Seismological and tectonic analysis, submitted to *Journal of Geophysical Research*, 1992), local strong motions and teleseismic *P* and *S* waves [*Wald*, 1992], regional surface waves (H. K. Thio, personal communication, 1992), and local *P-SV* and *P-SH* amplitude ratios (K. F. Ma, personal communication, 1992). The standard deviation to the mean of these solutions is less than 7°. Of greater interest, however, was the similarity of the waveforms at three of the equidistant stations indicating that a common Green's function was sufficient for use in the source inversion. Figure 2 compares the displacement data recorded at GSC, ISA, PFO, and SBC with displacement synthetics computed with an F-K integration method. The data were integrated to ground displacement from velocity within the frequency band from 0.005 to 7.0 Hz. The synthetics were computed up to 5 Hz using a slightly modified version of the standard southern California velocity model (SC, Table 1) commonly used to locate earthquakes. This model is based primarily on travel times from quarry blasts [*Hadley and Kanamori*, 1977] and teleseismic surface waves [*Hadley and Kanamori*, 1979]. The body wave portions of the records in Figure 2 are well modeled. Phases produced by discontinuities in the model are clearly identifiable in the data. The surface waves are also reasonably well modeled in terms of the dispersion, but they show the largest variation in timing. This is most apparent in the data recorded at SBC, where both the Love and Rayleigh waves are delayed by as much as 8 to 10 s. The complexity observed at SBC is likely due to the multipathing of energy through the Ventura basin. It should be noted, however, that many of the body wave arrivals predicted by the synthetics are observed in the SBC data [*Helmberger et al.*, 1993]. The similarity in waveform at the other stations, despite very different travel paths, suggests that this model may be appropriate for use over a wide area in southern California. Of course, it will not work everywhere due to differing degrees of two- and three-dimensional influences on wave propagation [see *Helmberger et al.*, 1992*a*]. This model also appears to be appropriate at larger ranges. Figure 3 shows a profile of vertical strike-slip synthetics computed for distances of 100 to 450 km. Note that the waveforms are very similar at neighboring distances. The largest differences are in the relative timing of specific phases. Figure 4 shows broadband data recorded at PAS for the December 3, 1991, Baja California (BAJA, distance of 345 km) and the October 24, 1990, Lee Vining (LeeV, distance 438 km) earthquakes. These events are discussed in detail in a later section, but it is interesting to compare the waveforms recorded for these earthquakes with the synthetics displayed in Figure 3. There is remarkable agreement between the body waves for this model and the data, considering that the energy from these two events traversed completely different paths. Thus it appears that the SC model has considerable applicability with respect to body waves from Baja California to northern California.

Inversion Method

To use inverse theory a measure of fitting error is needed to quantify the misfit of the model to the data. *Wallace et al.* [1981] used

$$E_i = 1 - \frac{\int_0^T [f_i(t) g_i(t)]\, dt}{\sqrt{\int_0^T f_i(t)^2 dt}\sqrt{\int_0^T g_i(t)^2 dt}} \qquad (1)$$

where the index i refers to the component, T is the length of seismogram considered, $f_i(t)$ is the data vector, and $g_i(t)$ is the Green's function vector. This parameterization is based on the zero-lag correlation coefficient and normalizes both the data and synthetics so that absolute amplitude information does not enter into the inversion. Another parameterization after *Liu*

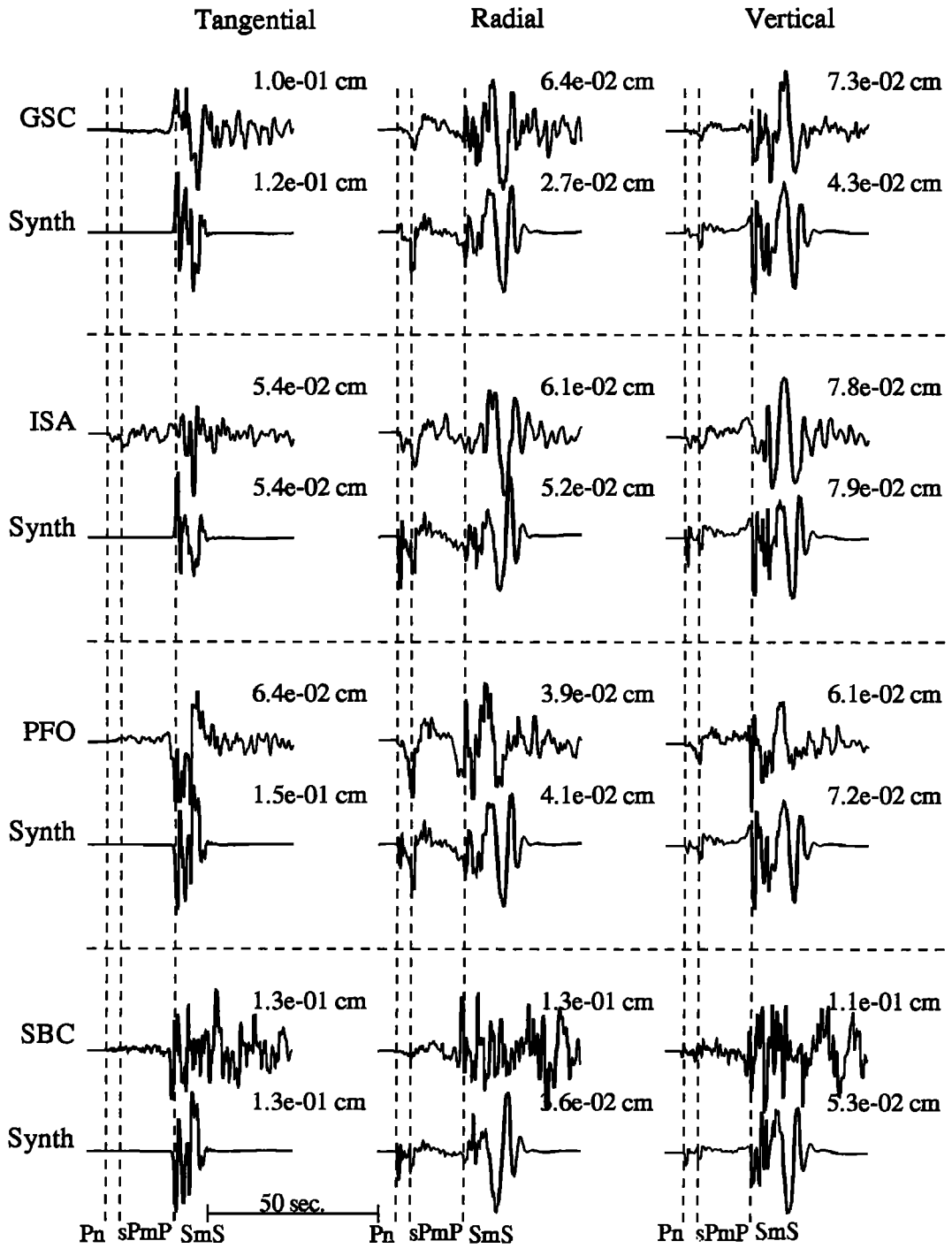

Fig. 2. Comparison of broadband displacement data recorded by TERRAscope and synthetic seismograms for the June 28, 1991, Sierra Madre earthquake. The amplitudes are ground displacement in centimeters. The focal mechanism determined by inversion of the three-component body waves [*Dreger and Helmberger*, 1991*a*] and a triangular source time function with a duration of 1 s were used in constructing the synthetics.

and Helmberger [1985] uses a fitting error not employing normalization.

$$E_i = \int_0^T [f_i(t) - g_i(t)]^2 \, dt \qquad (2)$$

This parameterization proved to be especially useful when trying to extract information about complex multi-source events. Although it is not discussed in this paper, we tested both parameterizations and found that including the amplitude information produced greater stability and more rapid convergence when using a single station because of the importance of the *SH* to *SV* amplitude ratio.

The Green's functions in (2) depend nonlinearly on strike, rake, and dip. The problem is linearized by writing the error as a sum of the error of an initial model and the error due to a perturbation to the model

$$E_i = e_i^0 + \delta e_i \qquad (3)$$

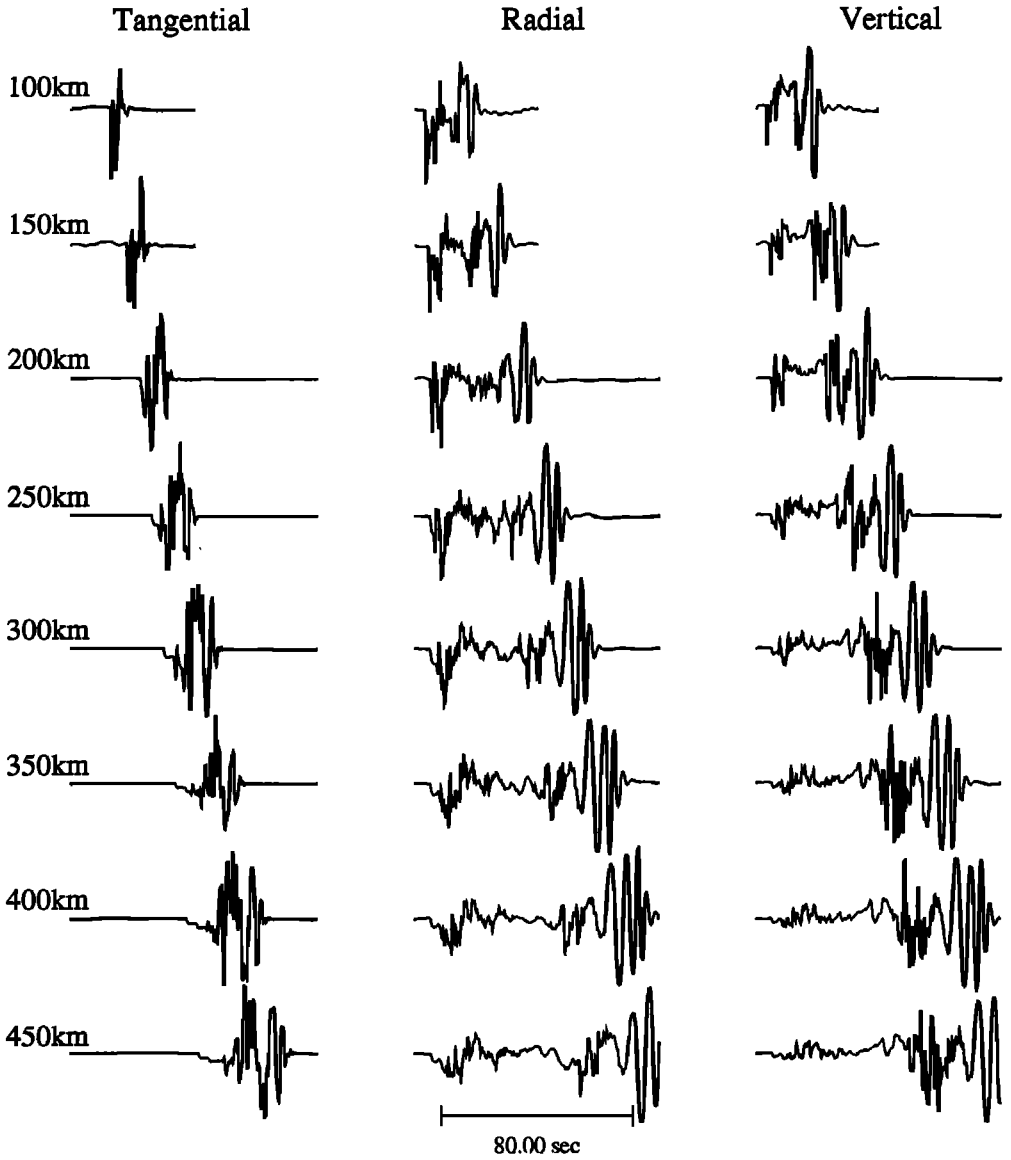

Fig. 3. Profile of broadband synthetic displacement seismograms for a vertical strike-slip fault. The synthetics were convolved with a triangular source time function with a duration of 1 s. The tangential and radial components were inverted to allow easier comparison with data shown in Figure 4. Because these synthetics are meant for waveform comparison alone and a generic focal mechanism was used, the amplitudes have been omitted from the plot.

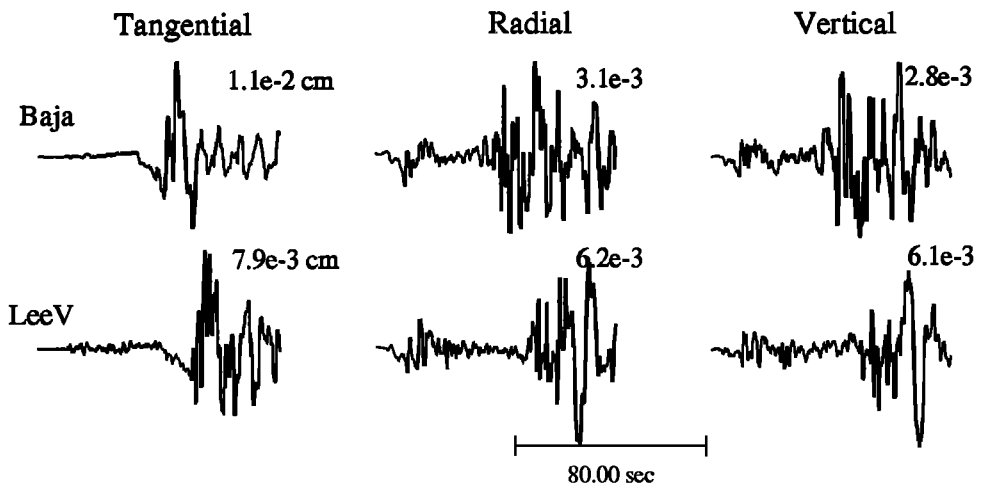

Fig. 4. The three-component displacement data recorded at PAS for the Baja California event (Baja, distance of 345 km) and the Lee Vining event (LeeV, distance of 438 km). Amplitudes are ground displacement in centimeters.

where δe_i is the error due to a perturbation and is defined as

$$\delta e_i = \frac{\partial e_i}{\partial \theta_j} \delta \theta_j. \quad (4)$$

Where $\frac{\partial e_i}{\partial \theta_j}$ is a matrix of partial derivatives of (2) with respect to the model parameters. The $\delta \theta_j$ are the perturbations to the initial model. By minimizing the sum of the squared error (3) with respect to the perturbations to the model parameters, a solution is found in which

$$\delta \theta_j = (A^T A + \delta I)^{-1} A^T e \quad (5)$$

Where $\delta \theta_j$ are the changes to the source parameters, e is the error matrix defined in (2), δI is a unit matrix damping term to stabilize the inversion, and A is a matrix of partial derivatives defined as

$$A = a_{ij} = \frac{\partial e_i}{\partial \theta_j}. \quad (6)$$

It is assumed that the δe_i terms are small. To arrive at a solution, a process of iteration from a starting model is used, where each successive iteration uses the preceding solution as a starting model. The δI term is chosen arbitrarily; however, we commonly use a value of 5% of the smallest diagonal term in the $A^T A$ matrix of the first iteration. We have not noticed any dependence of the solution on the choice of the damping term, only that it controls the size of the iterative step. The iterative procedure is continued until convergence is obtained. One of the problems with nonlinear inversions, however, is the fact that there may be some inherent dependence of the final solution on the starting model. A priori information can be used to help constrain the inversion, but for small earthquakes, earthquakes without good coverage, and historical earthquakes, a priori information may not be available. One way of determining if there is any dependence on the starting model is to use graphical means to examine the parameter space. For inversions involving many parameters this approach is prohibitively complex. The number of parameters in a source inversion, however, are relatively few. The approach taken here is to invert solely for strike, rake, and dip, and to use graphical means to determine the uniqueness and resolvability of the solutions. Since we iterate to a solution, each iteration provides a measure of the misfit for that solution. By using a number of starting models the error surface can be effectively mapped out and allow one to ascertain the uniqueness and resolvability.

In practice we low-pass filter both the data and Green's functions to minimize errors due to misalignment of the shorter-period arrivals. For the events discussed in this paper we filtered both the data and the synthetics with a Press-Ewing instrument response. Since surface waves are very sensitive to shallow, lateral heterogeneity [*Ho-Liu*, 1988; *Stead*, 1989], only the body waves are used. The whole body waveforms from the initial P wave to approximately the $S_m S$ phase are used, thereby inverting both the P waves and the S waves simultaneously. Although it is possible to weight each component individually, we normally weight all of the data traces equally. The seismic moment and source depth parameters are iteratively tested with the rms error (equation (2)), and for each value the mechanism that reduces the residuals is found.

Effects of Hypocenter Mislocation

It is useful to explore the effects of source mislocations on the inversion procedure using synthetic seismograms. We examined cases of both epicentral and vertical source mislocations (Figures 5*a* and 5*b*). Single- and multiple-station cases were considered. The synthetic data and Green's functions were processed in the same manner that has proven effective with real data. A low-pass filter was used to minimize errors due to misaligning the shorter period arrivals and only the body waves were used. The same velocity model was used to compute both the synthetic data and Green's functions with an F-K integration method. The synthetic data were given a source orientation of $\theta = 75°$, $\lambda = 45°$, and $\delta = 65°$.

Lateral mislocation. Figure 5*a* shows the assumed geometries. First, we examined the effect of mislocating the source 10 km in the radial direction (single-station case S1). Figure 6*a* shows the graphical representation of the parameter space. Each dot represents the error and the corresponding solution of a single iteration. The conjugate solution is also plotted for each iteration. Four starting models were used, and the inversion was permitted to iterate 50 times. Usually convergence was obtained within 10 iterations. Examination of the parameter space (Figure 6*a*) reveals that a mislocation in distance produced two global minima in strike and rake. These minima are due to the two nodal planes of a double-couple source. Rather pronounced local minima are also evident. In this case we could choose the correct solution because the differences in the residuals of the global and local minima are large. The global minima give a solution of $\theta = 80°$, $\lambda = 46°$, and $\delta = 60°$. A sample of the fits to the data is given in Figure 7.

Next, we examined the effect of mislocating the source 10 km in the tangential direction. The geometry is from station S2 to the source (Figure 5*a*). Figure 6*b* shows the graphical representation of the parameter space. In this case, only the global minima are observed, and the error reduction is over 5 orders of magnitude. The global minima give a solution of $\theta = 80°$, $\lambda = 48°$,

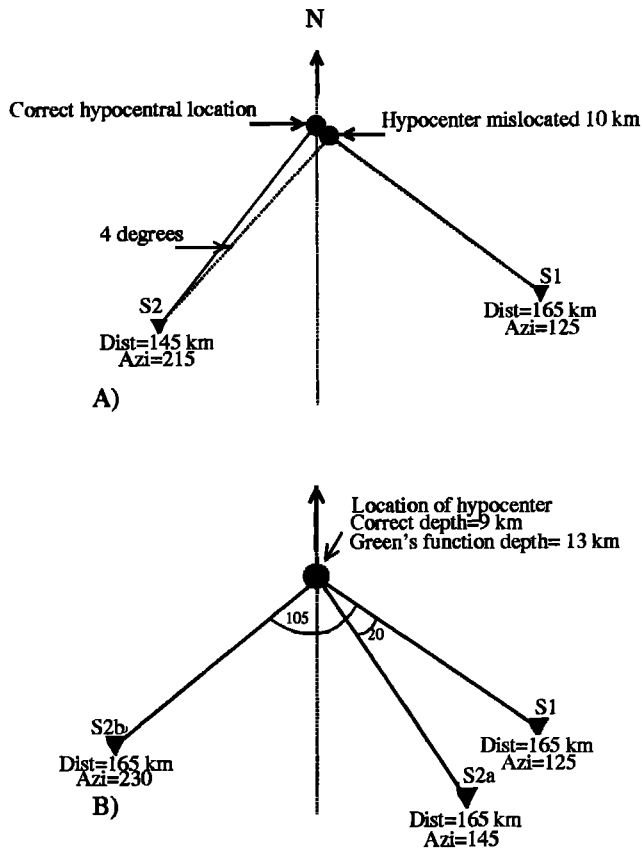

Fig. 5. (*a*) Diagram showing the station-source geometries used in the lateral mislocation sensitivity analysis. (*b*) Diagram showing the station-source geometries used in the vertical mislocation sensitivity analysis. Dist is distance, and Azi is azimuth.

and $\delta = 64°$ which is nearly the correct answer. The addition of a second station as displayed in Figure 5*a* improves the parameter space significantly (Figure 6*c*), in that the local minima observed in Figure 6*a* have disappeared. Both stations S1 and S2 were used in this test. The global minima yield a solution of $\theta = 79°$, $\lambda = 47°$, and $\delta = 62°$. It should be noted that while the local minima disappeared with the addition of a second station, there was a slight broadening of the global minima. This broadening is likely due to the two stations having slightly different error surfaces as is evident by comparing Figures 6*a* and 6*b*. The simultaneous inversion of the two stations describes the shared error surface. The parameter space also allow one to determine the uncertainties directly from the width of the minima.

Vertical mislocation. The synthetic data were generated in the same manner as the previous section except an incorrect source depth and correct distances were used. The mislocation in source depth was 4 km. Figure 5*b* shows the geometries tested. First, we tested the effects on a single station (S1). The 4 km mislocation in depth has dramatic effects on the parameter space (Figure 8*a*), in which a significant nonuniqueness is characterized by local minima in both strike and rake. In contrast to the previous example the residuals of the minima are nearly the same. The nonuniqueness occurs at a strike of 170°, 100° from the 70° and 130° from the 310° minima associated with the correct strikes of the double-couple source. Occasionally, with steeply dipping faults as many as four minima in strike can be observed due to the uncertainty in dip. For example, if the dip exceeds 90°, then the strike rotates 180° in our convention. The redundant minima are distinguished from nonuniqueness by the 180° separation and by a lack of nonuniqueness exhibited in the rake or dip parameter space. Note that the rake parameter space clearly shows the nonuniqueness as well. The lowest errors give a solution close to the starting solution, where $\theta = 73°$, $\lambda = 54°$, and $\delta = 65°$, but without additional a priori information it would not be possible to choose the correct solution based solely on the misfit error level. Figure 9 compares the waveforms for the two possible mechanisms. Note that the mechanisms are significantly different, yet the waveforms are remarkably similar.

Second, we used two stations with an aperture of 20° (S1 and S2a), representing an event occurring outside the array. Figure 8*b* shows the parameter space. The nonuniqueness observed in Figure 8*a* is removed with the addition of the second station, even though the aperture is small. This test yielded a solution of $\theta = 69°$, $\lambda = 35°$, and $\delta = 70°$.

Third, we used two stations with an aperture of 105° (S1 and S2b). Figure 8*c* shows the parameter space. The nonuniqueness is further removed, and the global minima are better defined. This test yielded a solution of $\theta = 69^0$, $\lambda = 44°$, and $\delta = 71°$.

Generally, these sensitivity tests show that source parameters can be obtained confidently from sparse data sets despite possible errors in source location. The tests described above examine 10 km lateral and 4 km vertical mislocations. It was found that these mislocations introduced small errors ($< 10°$) in the source mechanisms. Larger mislocations would, of course, introduce larger errors. The effect of vertical mislocations appears to be much stronger, which in fact is quite useful because it provides a means of constraining the source depth by both parameter space analysis and iteratively using the rms misfit error (equation (2)). The greater source depth sensitivity is due to the changes in relative amplitudes of initially upgoing versus downgoing energy, while the lateral mislocations do not significantly change the relative amplitudes, only the differential travel times.

One of the most important aspects of this method is the assumption that we know the velocity model. Several studies to date, which use local and regional three-component data, indicate that at longer periods, simple

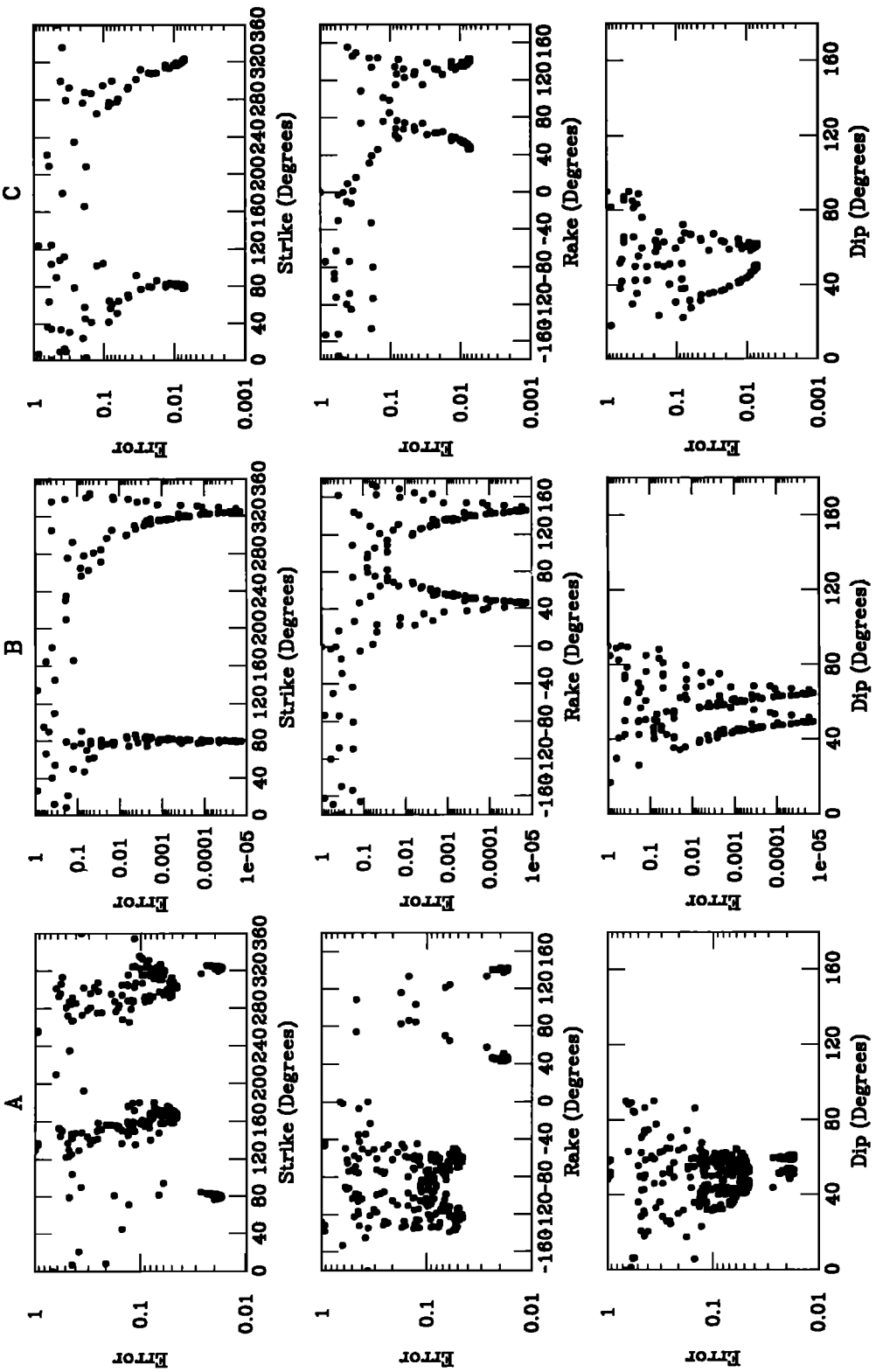

Fig. 6. Parameter space for lateral mislocation sensitivity tests. The iterative method of the inversion effectively maps the error surface. Each dot represents the error level and corresponding solution of a particular iteration. Both nodal planes of the double-couple are plotted for each iteration. (*a*) Parameter space for the strike, rake, and dip model parameters using only station S1 (Figure 5*a*) in the inversion. Note that there are several local minima on the error surface. (*b*) Parameter space using only station S2. This error surface only has the two global minima associated with the two nodal planes of the double-couple source. (*c*) Parameter space using both stations S1 and S2. The addition of a second station effectively removes the local minima observed in Figure 6*a*.

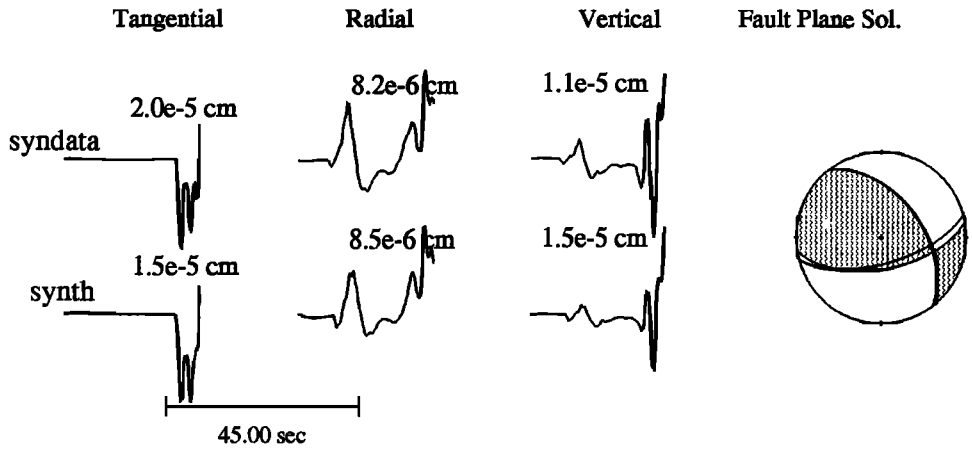

Fig. 7. Comparison of the synthetic data (syndata) and best fitting synthetics (synth) for the lateral mislocation sensitivity test (Figure 6a). Both the Green's functions and synthetic data were computed with an FK integration code. They were processed by convolving with a Press-Ewing instrument response and truncating the records before the arrival of the fundamental surface wave. The data were computed for distances of 155 and 145 km for the S1 and S2 source station pairs, respectively. The Green's functions were computed for distances of 165 and 145 km, respectively. Both the synthetic data and the Green's functions were computed for a source depth of 11 km. The focal mechanism shows the result of the inversion (shaded) and the correct solution (unshaded).

plane layered velocity models derived from travel time studies appear to be adequate in explaining the long-period data. Using an inappropriate velocity model can have significant effects on the final result, as discussed later, when inverting the Lee Vining data.

APPLICATIONS

Although the technique has been applied to numerous events, we will limit this particular study to two events which serve to demonstrate its usefulness. The first event occurred in northern Mexico and the second in northern California, roughly in opposite directions and well outside the TERRAscope array.

December 3, 1991, Baja Event

On December 3, 1991, a moment magnitude 5.1 earthquake occurred at 31.75°N and 115.83°W (J. Garcia of the Centro de Investigacion Cientifica y de Educacion Superior de Ensenada, B. C. (CICESE), written communication, 1991), approximately 20 km north of the San Miguel fault. This event was recorded by all six of the TERRAscope stations (see Figure 1) at distances ranging from 215 km to approximately 515 km with an aperture of approximately 40°. Figure 10 shows the displacement data recorded at PAS (distance of 345 km) and the seismograms filtered through the 0.8 s torsion (WASP), 6.0 s torsion (WALP), and Press-Ewing (3090) instruments. The displacement data were obtained by integrating the broadband velocity data within the frequency band from 0.005 to 7.0 Hz. The simulated instrumental seismograms were computed by convolving the displacement records with the instrument response of the traditional instrumentation. Several features to take note of in the broadband data are the very pronounced onset of S_n on the tangential component, the long-period P_{nl} waveform, and the lack of a coherent Raleigh wave on the radial and vertical components. For the most part, the energy propagated through the Peninsular Ranges; however, the last 50 km traversed the Los Angeles basin structure which accounts for the complexity observed in the surface waves. Note the relative simplicity of the 3090 waveforms. The large instrumental amplitudes indicate that these records would have been clipped on the traditional instrumentation. Figure 11 shows the displacement, 3090, WALP, and WASP data recorded at PFO. Compared to PAS the Rayleigh waves are more coherent. The long-period P waves are the result of interfering P_{nl} and upper crust PL waves.

We used the simulated 3090 data recorded at PAS (Figure 10) and PFO (Figure 11) in the inversion. These stations were located at distances of 345 and 215 km and azimuths of 321° and 344°, respectively. Inversions were performed using both a single station (PAS) and two stations. F-K synthetics previously computed for a standard crustal model (SC, Table 1) were used. Five source depths were tested. A triangular source time function with a width of 1 s was assumed. In addition, only the body waves were used to eliminate the problems with the surface waves as discussed earlier.

The inversion using only PAS produced unique results and yielded a solution where $\theta = 305°$, $\lambda = 163°$, $\delta = 80°$, and $M_o = 5.2 \times 10^{16}$ N m; the source depth was 11 km. The seismic moment and source depth parameter space are plotted in Figures 12*a* and 12*b*. Both show well-defined global minima. The orientation parameter space is shown in Figure 13. Two of the four minima in

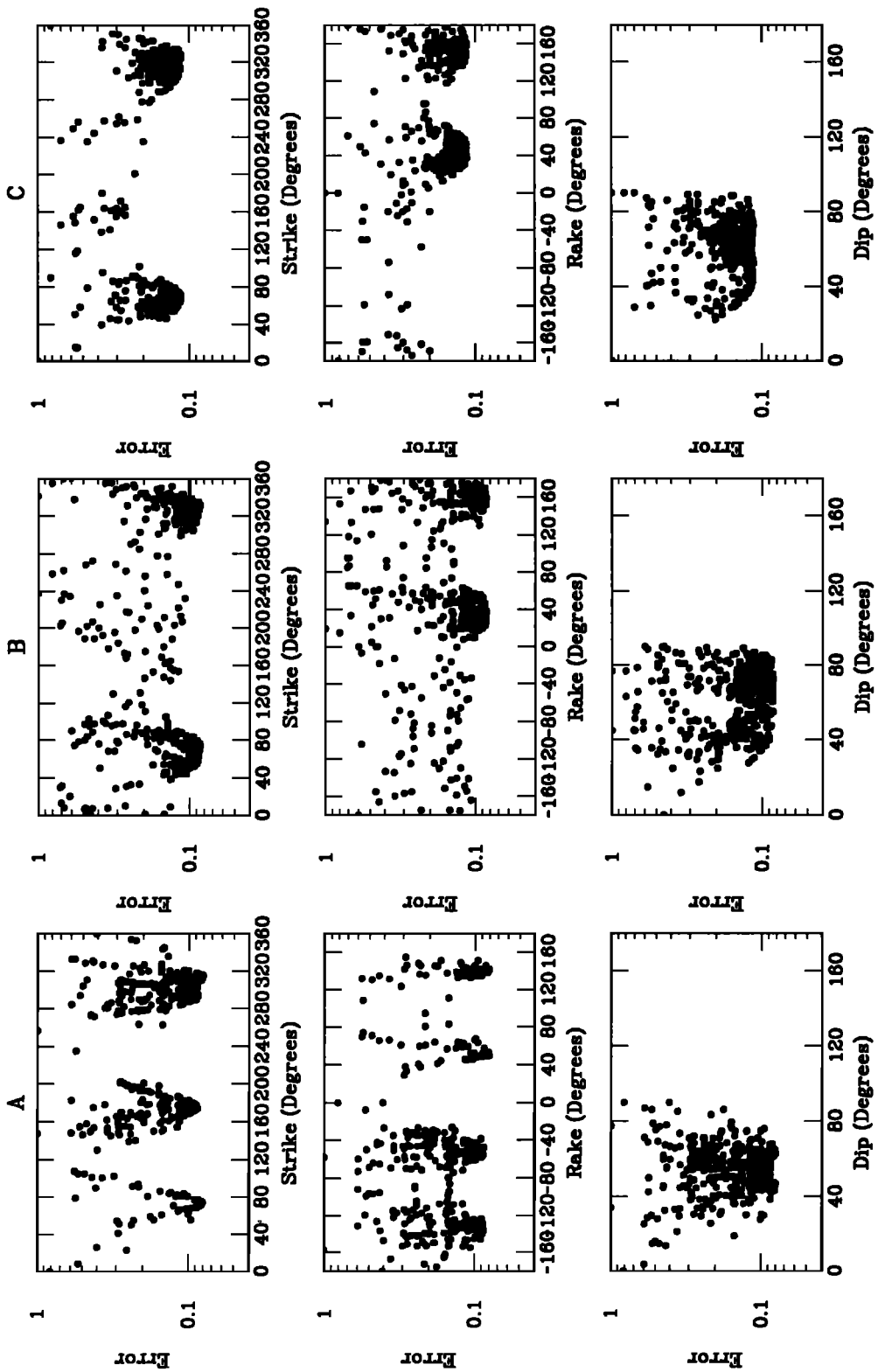

Fig. 8. Parameter space for vertical mislocation sensitivity tests. See Figure 6 for a description of the plot. (*a*) Parameter space for the strike, rake, and dip model parameters using only station S1 (Figure 5*b*) in the inversion. The error surface is characterized by several local minima with similar residuals indicating a nonunique solution. (*b*) Parameter space using both stations S1 and S2a. (*c*) Parameter space using both stations S1 and S2b. The addition of the second station effectively removes the nonuniqueness.

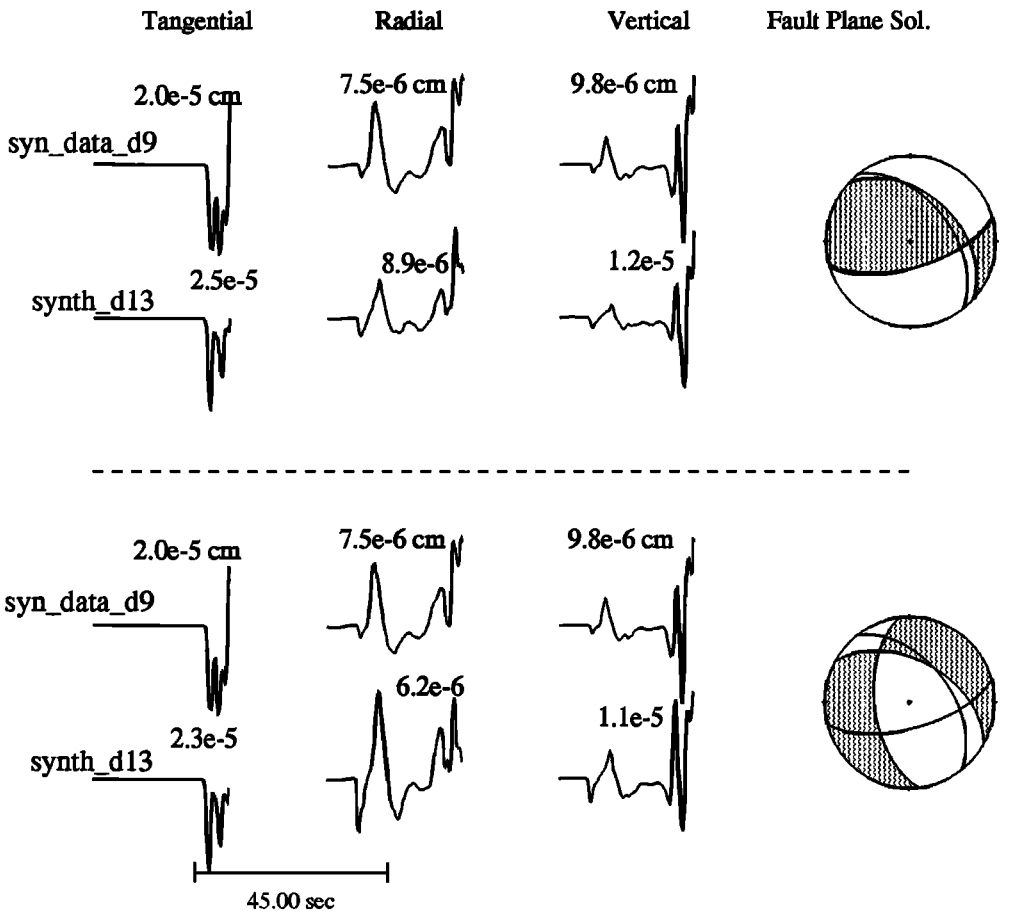

Fig. 9. Comparison of synthetic data (syn_data_d9) and synthetics (synth_d13) computed with the two nonunique solutions observed in Figure 8a. See Figure 7 for details of Green's function and synthetic data processing. The data were computed with a source depth of 9 km, while the synthetic was computed with a source depth of 13 km. Both the synthetic data and Green's functions were computed for a distance of 165 km. Only station S1 was used (Figure 5*b*). The focal mechanisms show the results of the inversion (shaded) and the correct solution (unshaded). Note that despite the radically different focal mechanisms the waveforms are strikingly similar.

the strike parameter space are redundant (i.e., 180° separated), the other two represent the two nodal planes of the assumed double-couple source. The parameter space shows that unique results were obtained with a single station. The uncertainties in this solution are less than 10° for each parameter. However, with this data alone it is not possible to determine which plane actually slipped during the earthquake. The two-station inversion produced very similar results with $\theta = 119°$, $\lambda = 191°$, and $\delta = 78°$. As before, a seismic moment of 5.2×10^{16} N m and a 11 km source depth produced the lowest residuals. The single-station (M1) and double-station (M2) results are plotted in Figure 1 for comparison. The largest difference between these solutions is about 22° in the dip of the northwest trending nodal plane. Figure 14 shows the waveform fits obtained by the inversion. There is good agreement in both waveform and amplitude. Note that the *SH* waves have opposite polarities at the two stations. The polarity of *SH* waves recorded at SVD (azimuth of 336° and distance of 286 km) is the same as at PAS indicating that the *SH* node is located between 336° and 344°. It should also be noted that the data recorded by SBC at a distance of 469 km and an azimuth of 308° indicate that the *P-SV* waves (P_{nl}) are nodal, supporting the results obtained by inverting PAS and PFO data. The location of this event as determined by CICESE places it approximately 20 km north of the San Miguel fault. In 1956 a $M_L = 6.5$ earthquake occurred on the San Miguel fault and broke the surface. The mechanism we obtained for the 1991 earthquake is consistent with the surface break observed after the 1956 event [*Shor and Roberts*, 1958].

Figure 15 shows the displacement, 3090, WALP, and WASP synthetics predicted for PAS by the source parameters obtained by inverting the 3090 body waves. In comparing the synthetics (Figure 15) with the data (Figure 10) we find that there is good agreement with the body waves for the displacement, 3090, and WALP records. At shorter periods (WASP records) the fit is not as good because the simple model fails to produce the complexity observed in the data, especially the level of *SV* energy on the radial component. We point out,

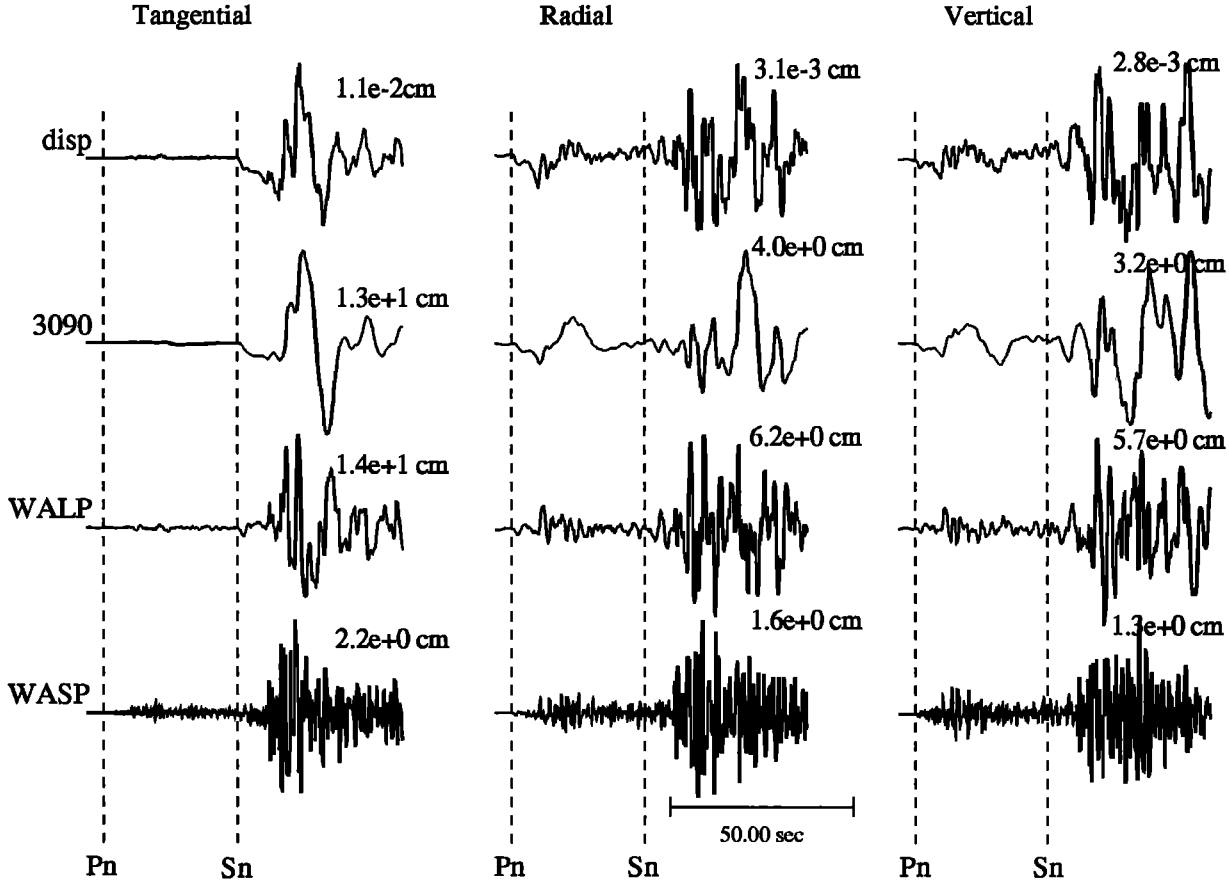

Fig. 10. Three-component displacement and simulated Press-Ewing (3090), 6 s torsion (WALP), and 0.8 s torsion (WASP) instrument records of the December 3, 1991, Baja California event (M_w = 5.1) recorded at PAS. The simulated instruments were derived by convolving the displacement data with the appropriate instrument response. Ground displacement and instrumental amplitudes are shown in centimeters.

however, that many of the arrivals from major discontinuities in the model seem to be observed in the short-period data especially on the tangential component, indicating that although lateral heterogeneity is a factor, the major body phases dominate. Notably, S_n has a particularly sharp onset for this path and is observed at shorter periods (e.g., WALP and WASP) in agreement with the synthetics shown in Figure 15. This suggests that the sharpness of the Moho discontinuity in model SC is appropriate along the path from Baja to PAS.

October 24, 1990, Lee Vining Event

The October 24, 1990, Lee Vining event was located at 38.05°N and 119.12°W, near Lee Vining, California at a depth of about 11.5 km [*Horton and Depolo*, 1992]. At the time of this event only two of the TERRAscope stations were installed. This earthquake was well recorded by the GSC (distance=365 km, azimuth=145°) and PAS (distance=438 km, azimuth=169°) stations. Figure 16 compares the displacement, 3090, WALP, and WASP data recorded at PAS. The data were processed in the same manner as the Baja data with the exception that the band-pass corner frequencies were 0.02 and 7.0 Hz. The tangential motions are plotted directly above the radial and vertical motions to emphasize the clean separation of the (*P-SV*)-(*SH*) systems of motion. Note, however, that the separation tends to break down in the WASP bandwidth. As in the Baja example, the waveforms are well ordered in that they are composed of phases that can be modeled using simple one-dimensional plane layered models. This is especially true for the long-period phases such as P_{nl}, and and S_n. Note that while S_n is clearly identifiable in the displacement and 3090 records, it is not a distinct phase in the WALP and WASP data. This contrasts with what was found for the Baja event and probably represents a fundamental difference in the sharpness of the Moho for this path. In addition, the Rayleigh wave recorded at PAS for this event is more coherent than that for the Baja event. In contrast to the seismograms recorded at PAS those for GSC have a lack of coherent energy on the radial and vertical components suggesting that this station is near a *P-SV* node. Furthermore, the tangential component motions are 4 and 6 times larger than the radial and vertical component motions, respectively.

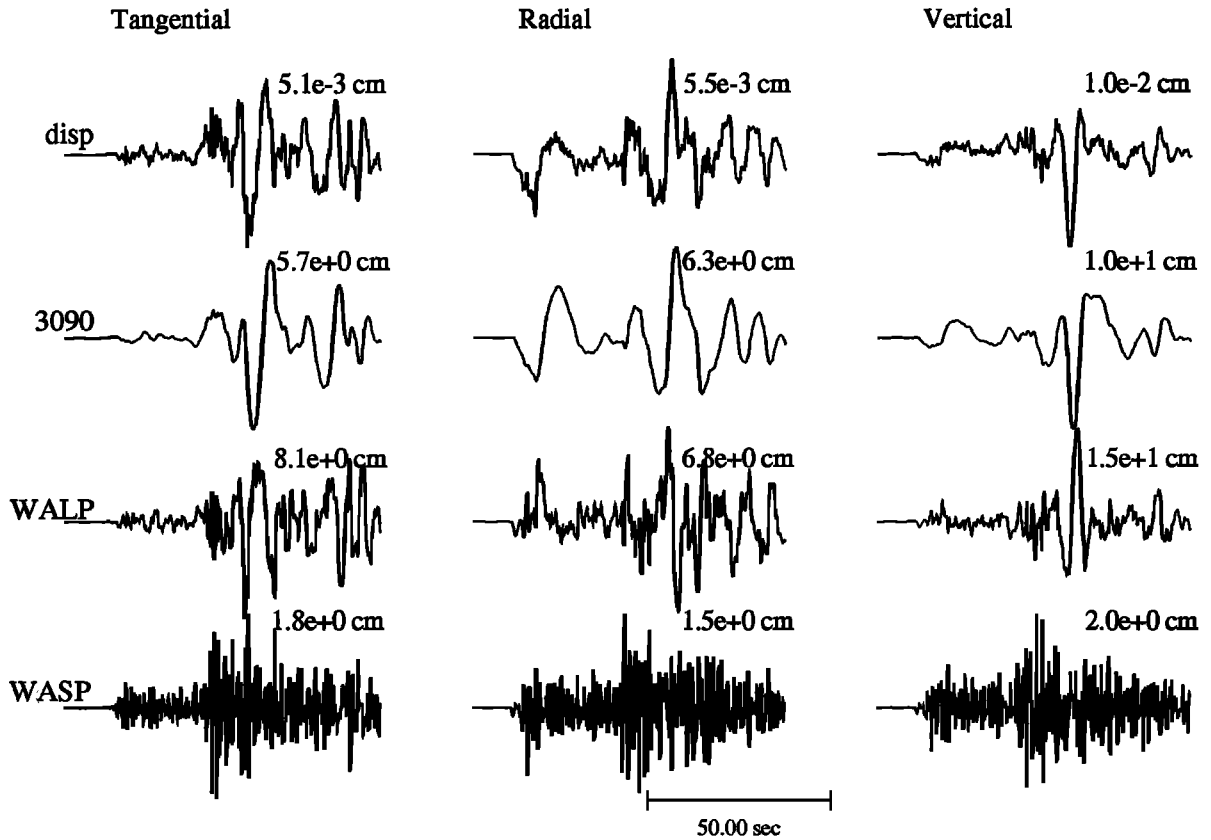

Fig. 11. Three-component displacement and simulated Press-Ewing (3090), 6 s torsion (WALP), and 0.8 s torsion (WASP) instrument records of the December 3, 1991, Baja California event (M_w = 5.1) recorded at PFO. The simulated instruments were derived by convolving the displacement data with the appropriate instrument response. Ground displacement and instrumental amplitudes are shown in centimeters.

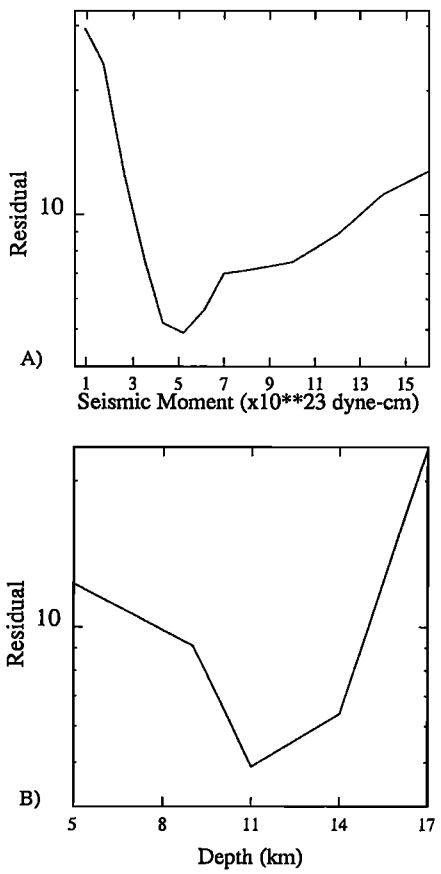

We inverted the 3090 body waves recorded at PAS and GSC using three different velocity models. The first model was the standard southern California velocity model (model SC), used to invert the Baja data. The second model was used by *Jones and Dollar* [1986] (model JD) to explain travel times of Sierran earthquakes recorded in southern California. The third is a layer over a half-space (model LH) approximation to the JD model. The models are listed in Table 1. A triangular source time function with a duration of 1 s was assumed We performed single-station inversions using the PAS data and found that the JD and LH models produced nonunique results, while unique results were obtained with the SC model. The parameter space were better defined with the inclusion of the GSC data, however. Table 2 lists the solutions obtained with the three models using both stations. Figure 17 shows the parameter space for these calculations. As was the case for the Baja event two of the four minima in the

Fig. 12. (*a*) Seismic moment parameter space of the single-station (PAS) inversion of the 3090 body waves. The lowest rms error was obtained with a seismic moment of 5.2×10^{16} N m. (*b*) Source depth parameter space. Five depths (5, 8, 11, 14, and 17 km) were tried. The minimum corresponds to a source depth of 11 km.

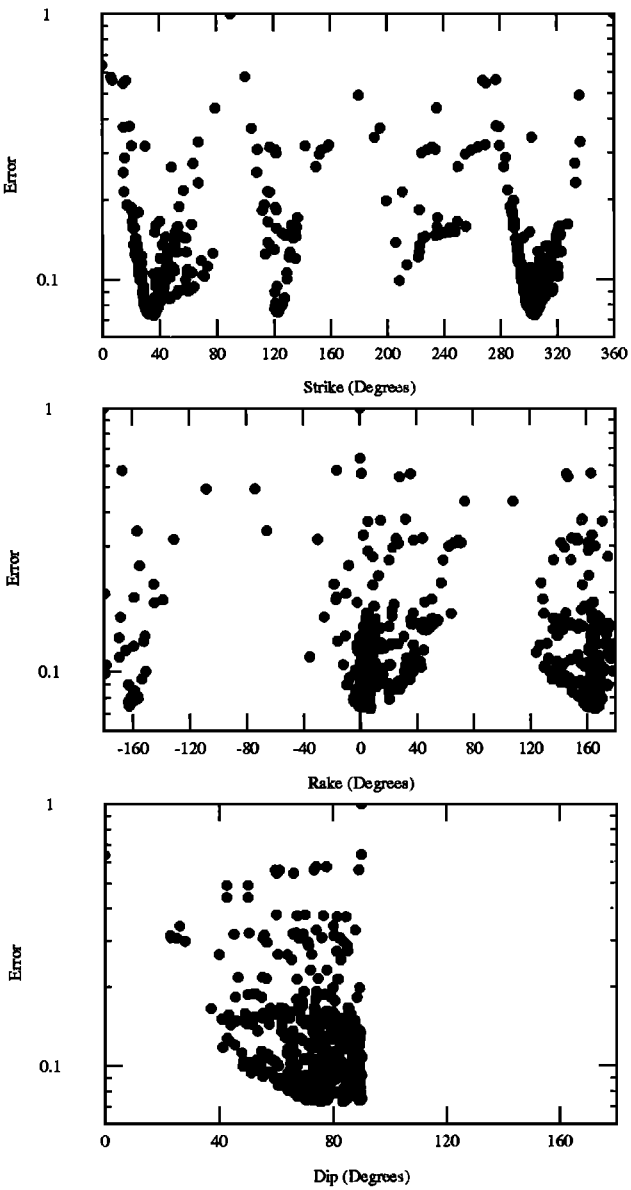

Fig. 13. Strike, rake, and dip parameter space of the single-station (PAS) inversion. The minima give a solution of $\theta = 305°$, $\lambda = 163°$, and $\delta = 80°$. Two of the four minima in strike are redundant (i.e., 180° separated). The other two correspond to the values of the two nodal planes of a double-couple source. The uncertainties determined from the width of the minima at the greatest error reduction indicate that they are less than 10°.

strike parameter space are redundant, and the remaining two correspond to values describing the two nodal planes of a double-couple source. It should be noted that the minima in Figure 17 differ from those for the Baja event (Figure 13) in that they are flat and broad. The width of the minima represent the uncertainty in the solutions, which in this case are about 20° for each parameter regardless of which velocity model is used. The broader minima obtained for this event probably represent problems with the velocity models used, and perhaps differences in crustal structure to each station. Figure 18 compares the 3090 data with synthetics computed for these solutions, and generally the waveforms are very similar and agree well with the data.

The average solution obtained from the three inversions using different velocity models is $\theta = 323 \pm 2°, \lambda = 174 \pm 17°, \delta = 81 \pm 2°$, and $M_o = (7.7 \pm 1.5)\, x\, 10^{16}$ N m. The uncertainties are the standard deviation from the mean of the solutions listed in Table 2. A rather large uncertainty exists for the rake parameter, but it is possible to distinguish that a strike-slip fault ruptured. Our solution compares reasonably well with the results of *Clark et al.* [1991] with respect to strike but poorly in terms of rake and dip. They find the northwest striking fault plane dipping west with a significant normal component of motion. They use P wave first-motions but do not have good azimuthal coverage, and most of their P wave picks are at P_n distances. Our results compare better with the P wave first-motion results of *Depolo and Horton,* [1991]. Their study had better azimuthal coverage and used some local distance stations. They report a mechanism striking 330° with a dip of 90° and a rake of 160°. Their rake is also somewhat poorly constrained. The depth of this event from first-motion data is approximately 11.5 km [*Horton and Depolo*, 1992]. Depth sensitivity curves of the type displayed earlier in Figure 12 do not show definitive minima, indicating a lack of resolution. Including the surface wave data could improve source depth determinations, but, as Figure 19 shows, the three models, while producing very similar body waves, generate substantially different surface waves. Adding the surface wave data in our inversion methodology will be addressed in future efforts.

Discussion and Conclusions

In this paper we addressed the issue of source retrieval from high-quality but limited data sets. We demonstrated that at long periods, regional structure is sufficiently well understood to estimate source parameters with very few stations. How few depends on the situation, but our various sensitivity tests suggest that one station will suffice in many situations. Although not discussed in this paper, horizontal mislocations of up to 15 km generally did not degrade the inversion results for the Baja event [*Dreger*, 1992]. The synthetic sensitivity analysis of vertical mislocations revealed that the long-period, regional body waves are sensitive to source depth because of changes in relative amplitudes of initially upgoing and downgoing energy and are therefore useful in source depth determinations. The inversion of the Baja data showed this to be the case, whereas the Lee Vining event had poor depth resolution. Problems associated with hypocenter mislocations, such as nonuniqueness, disappeared with the addition of a sec-

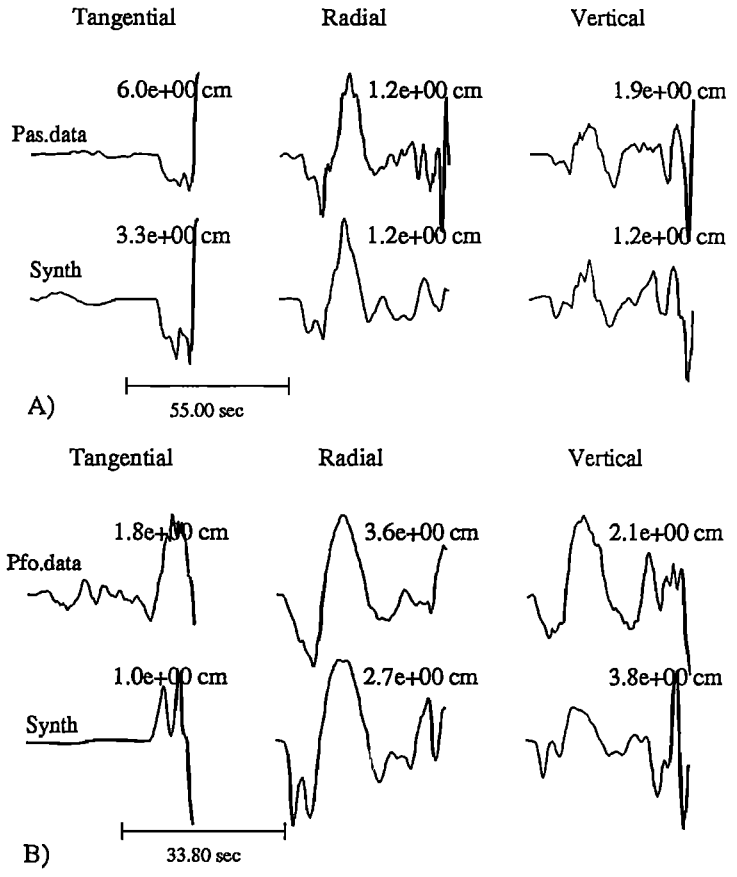

Fig. 14. Comparison of 3090 data and synthetics for stations (*a*) PAS and (*b*) PFO. The synthetics were computed with a strike of 119°, a rake of 191°, a dip of 78°, and a seismic moment of 5.2×10^{16} N m. Instrumental amplitudes in centimeters are shown.

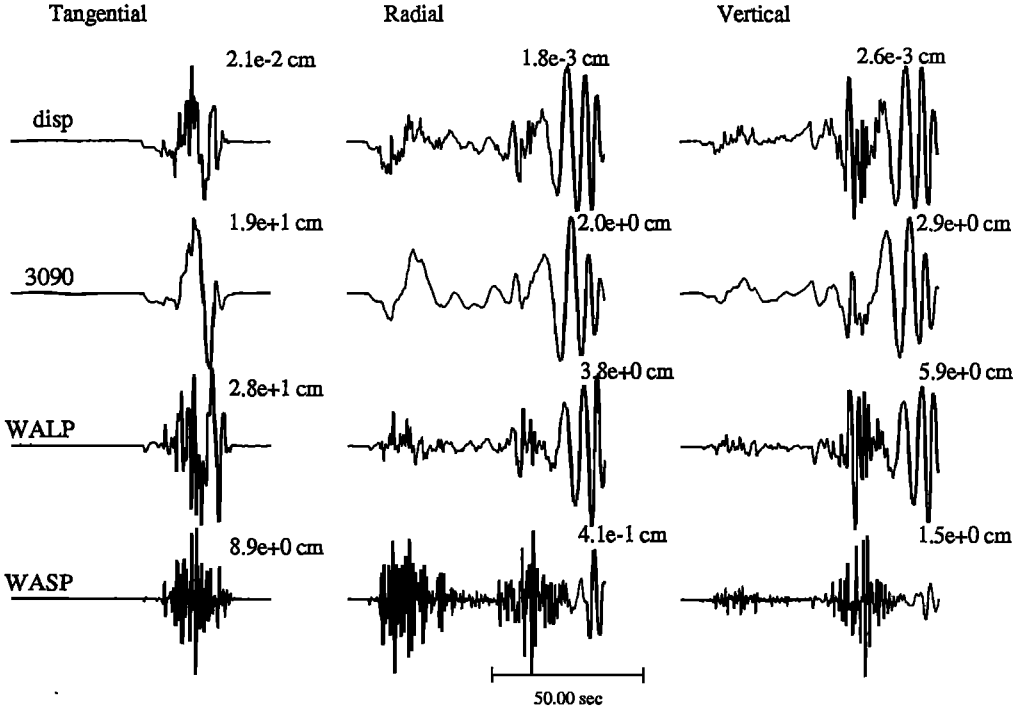

Fig. 15. Three-component, whole waveform displacement, 3090, WALP, and WASP synthetics computed with the mechanism obtained by inverting only the PAS 3090 body waves. For the tangential component the comparison with the data (Figure 10) reveals that this model is adequate to frequencies as high as 1 Hz. The lack of significant short-period SV waves on the radial component illustrates the shortcomings of a one-dimensional velocity model.

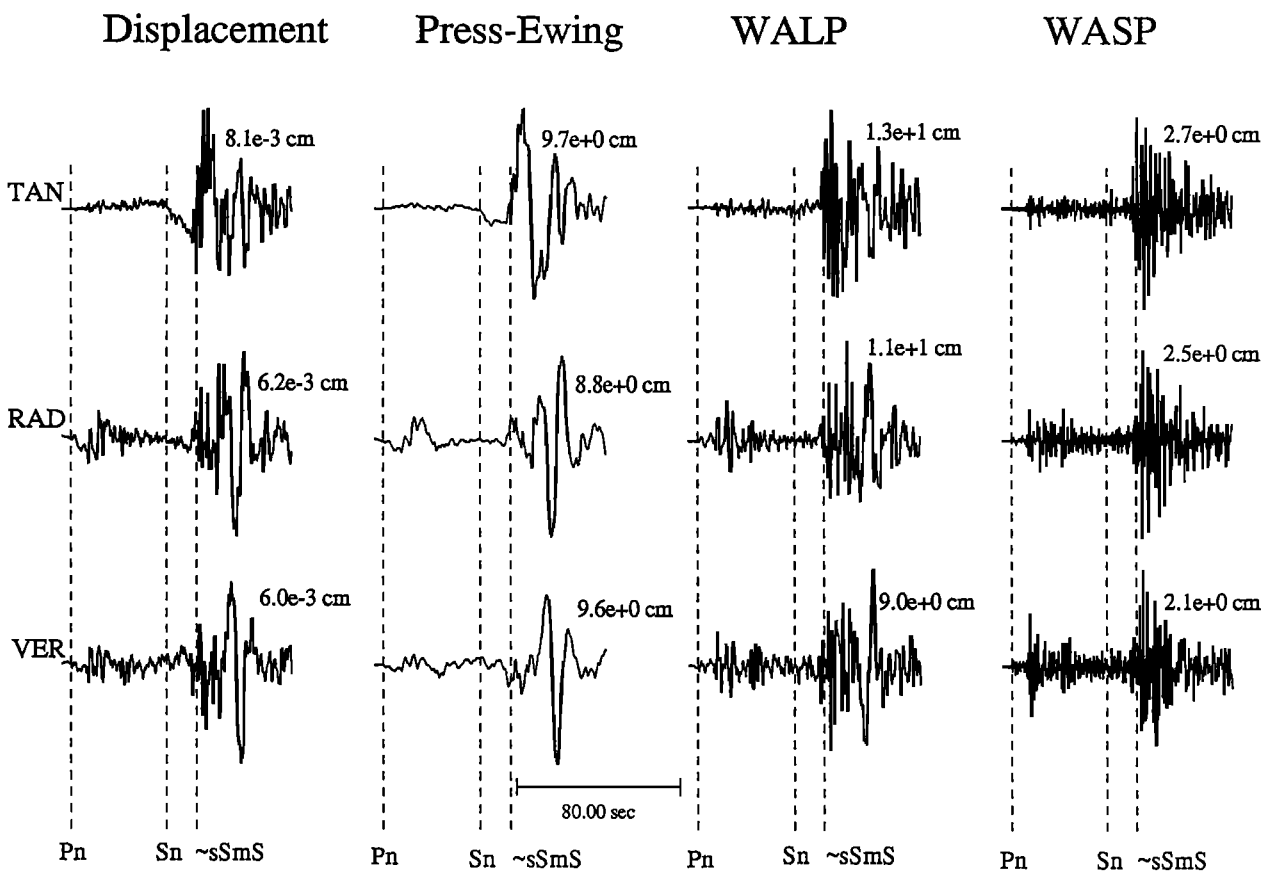

Fig. 16. Comparison of the displacement, Press-Ewing (3090), WALP, and WASP data recorded at PAS for the October 24, 1990, Lee Vining earthquake (M_w = 5.2). Ground displacement and instrumental amplitudes are shown in centimeters.

TABLE 1. Velocity Models

	V_p, $\frac{km}{s}$	V_s, $\frac{km}{s}$	ρ, $\frac{kg}{m^3}$	Z,km
SC Model	5.50	3.18	2400	0.0
	6.30	3.64	2670	5.5
	6.70	3.87	2800	16.0
	7.80	4.50	3000	35.0
JD Model	5.10	3.02	2500	0.0
	5.80	3.45	2650	2.0
	6.20	3.65	2730	8.0
	6.90	3.85	2900	22.0
	7.90	4.40	3210	36.0
LH Model	5.90	3.45	2670	0.0
	7.80	4.30	3300	33.0

Z is the depth to the top of a layer. Model SC is a slightly modified version of the model routinely used determine source locations in southern California. The JD model was used by *Jones and Dollar* [1986] to locate Sierran earthquakes recorded in southern California. The LH model is a layer over a half-space approximation to the JD model.

TABLE 2. Lee Vining Solutions Obtained With Each of the Three Velocity Models

Model	θ	λ	δ	M_o,N m
SC	322	162	83	9×10^{16}
JD	325	193	80	8×10^{16}
LH	321	167	80	6×10^{16}

Uncertainties on the strike (θ), rake (λ), and dip (δ) model parameters are approximately 20° for each velocity model. The uncertainties are determined by the width of the minima in Figure 17. The models are described in the Table 1 note.

ond station. Another important result of these tests was that good azimuthal coverage is not required when three-component data are used. This result was confirmed by both applications where the aperture between stations was only about 24°, yet stable results were obtained.

The assumption that the velocity model is known is an important one. The analysis presented in this paper shows that even with radically different velocity models (SC and JD compared to LH), the long-period body waves (primarily P_{nl} and S_n) are insensitive to lateral and vertical heterogeneity but are sensitive to source orientation. For example, the Baja and the Lee Vining events recorded at PAS at distances of 345 and 438 km have remarkably similar waveforms. Recall Figure 4, where it was shown that despite the 93 km difference in range and completely different travel paths, the body waves are very similar in waveform; of course, there are large differences in the relative timing of the phases. If the Sierra Madre earthquake is included in the discussion we find that model SC explains the data very well from 160 to 438 km for a variety of azimuths. Although regional distance P_{nl} and long-period SH and SV waves are relatively insensitive to upper crustal structure, the

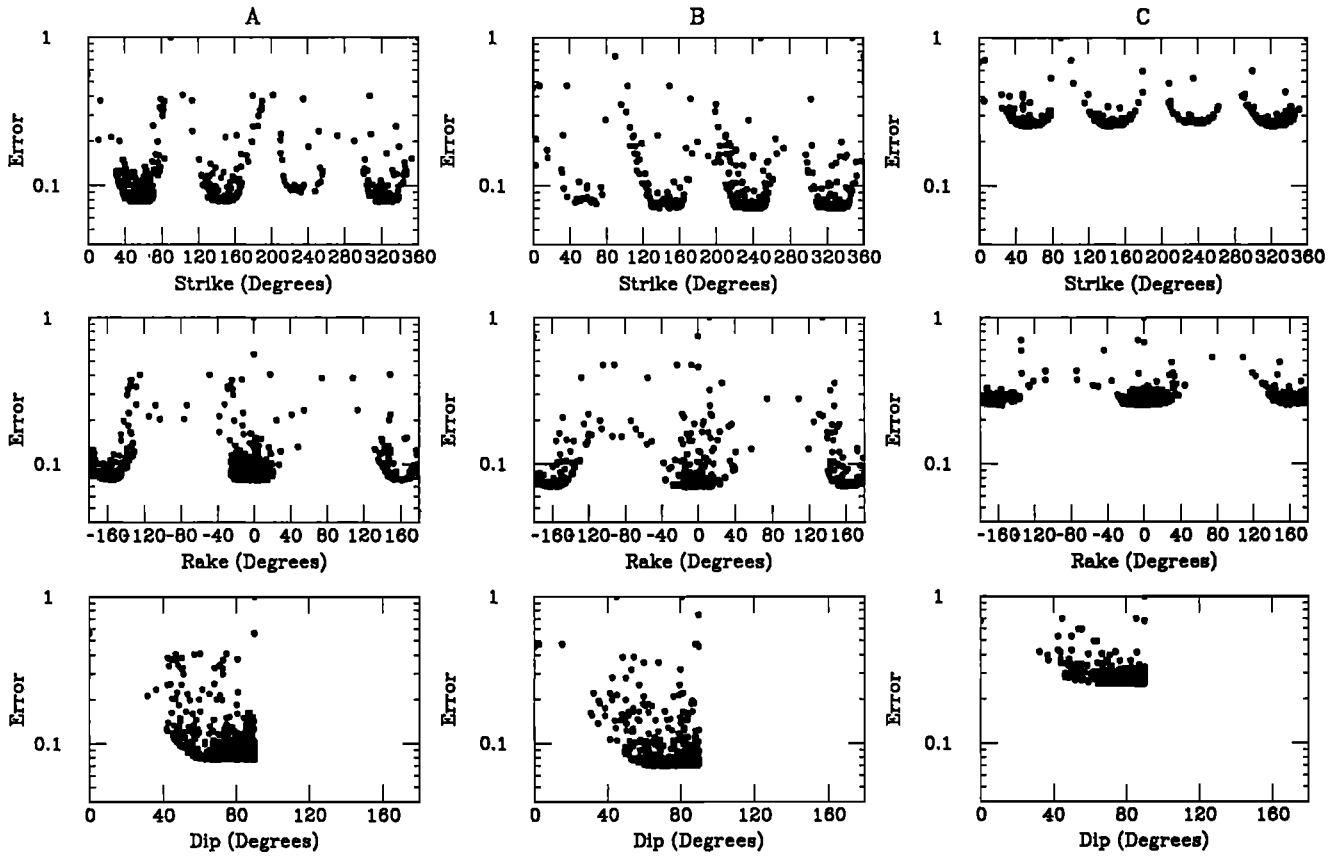

Fig. 17. Strike, rake, and dip parameter space for an inversion using both the PAS and GSC stations and the (*a*) SC, (*b*) JD, and (*c*) LH velocity models (Table 1). See Table 2 for the solutions. The shape of the minima are broader and flatter than those found for the Baja event (Figure 13). The uncertainties estimated from the width of the minima are approximately 20° for each parameter independent of velocity model.

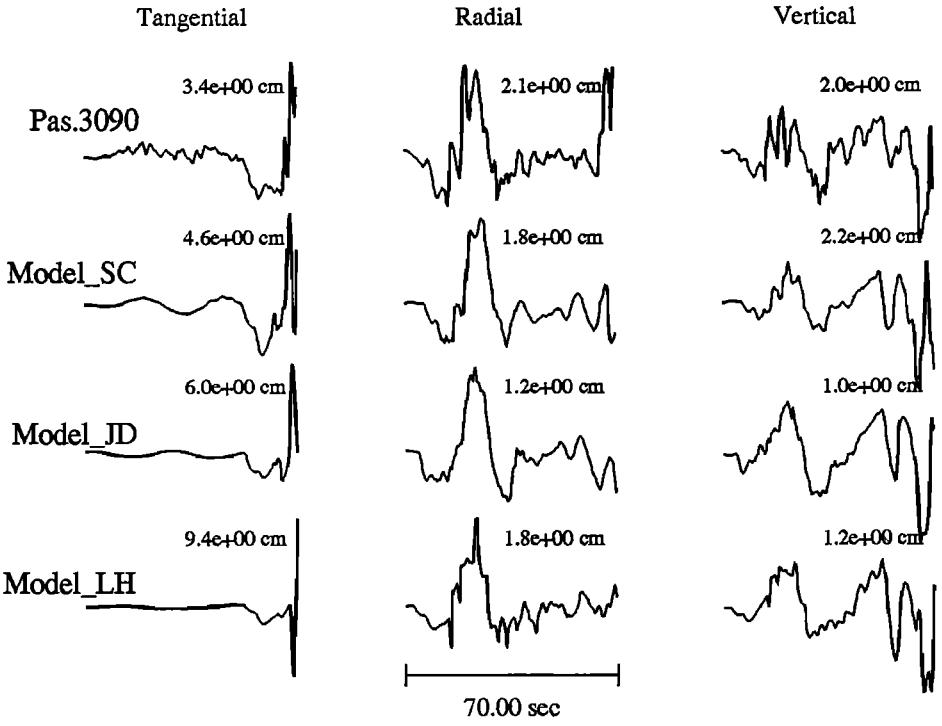

Fig. 18. Comparison of 3090 body waves recorded at PAS and the best fit synthetics using the SC, JD, and LH velocity models.

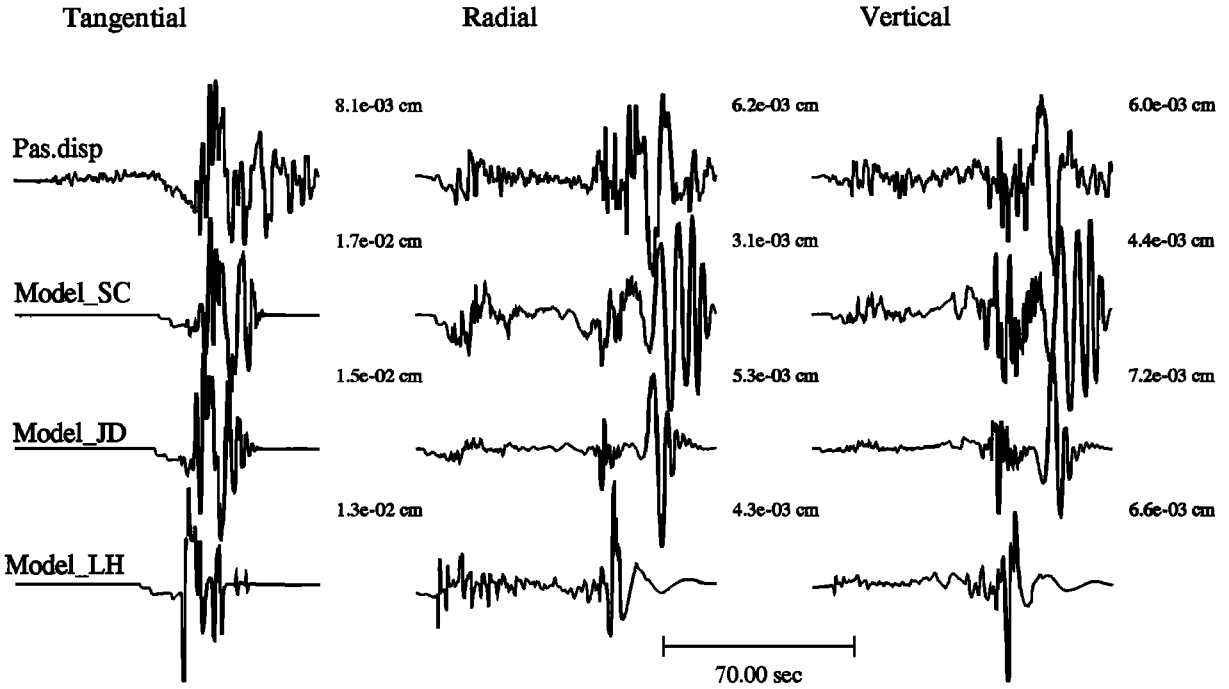

Fig. 19. Comparison of whole waveform displacement data recorded at PAS and synthetics for the SC, JD, and LH velocity models. Note that while the body waves are similar for each of the models, the surfaces waves that are generated differ markedly.

lowest errors in the Lee Vining inversions were obtained with models SC and JD which include upper crustal interfaces. In fact, at near-regional distances (100 to 300 km) the *PL* waves propagating along shallow interfaces are observed and have significant amplitude in the data.

In conclusion, we have demonstrated that regional, three-component, long-period body waves are stable enough to invert for source parameters. The signal-to-noise ratios of the data used in this study are very good (greater than 10). It should be possible to invert for source parameters for events larger than M_w=4.2 at these distances. To recover source parameters for smaller earthquakes, better Green's functions that explain the shorter-period propagation characteristics are needed. Some preliminary results in modeling regional waves at shorter periods appears promising (compare, for example, Figures 10 and 15) and will be addressed in future efforts. Surface waves are clearly the largest arrivals in the regional data but are sensitive to lateral heterogeneity and shallow crustal structure. Progress has been made by calibrating certain paths for surface wave propagation [*Patton and Doser*, 1988; *Beck and Patton*, 1991; *Thio and Kanamori*, 1991] to make better use of this portion of the regional seismograms.

Acknowledgments. We would like to thank Chandan Saikia for providing the F-K integration program used to compute the synthetic seismograms. David Wald and Egill Hauksson reviewed an early version of the manuscript. This research was supported by the Advanced Research Projects Agency of the Department of Defense and was monitored by the Air Force Geophysics Laboratory under the contract F19628-89-K-0028. This is contribution 5051 of the Division of Geological and Planetary Sciences, California Institute of Technology.

REFERENCES

Beck, S. L., and H. J. Patton, Inversion of regional surface-wave spectra for source parameters of aftershocks from the Loma Prieta earthquake, *Bull. Seismol. Soc. Am., 81,* 1726-1736, 1991.

Clark, M. M., D. P. Hill, K. R. Lajoie, A. R. Lindy, D. H. Oppenheimer, and J. C. Yount, Mono Basin earthquake of October 23, 1990, Internal Report, U.S. Geol. Surv., Menlo Park, Calif., 1991.

Depolo, D. M., and S. P. Horton, A magnitude 5.0 earthquake near Mono Lake, California, *Seismol. Res. Lett., 62,* 52, 1991.

Dreger, D. S., Modeling earthquakes with local and regional broadband data, Ph.D. thesis, Calif. Inst. of Technol., Pasadena, 1992.

Dreger, D. S., and D. V. Helmberger, Broadband modeling of local earthquakes, *Bull. Seismol. Soc. Am., 80,* 1162-1179, 1990.

Dreger, D. S., and D. V. Helmberger, Source parameters of the Sierra Madre earthquake from regional and local body waves, *Geophys. Res. Lett., 18,* 2015-2018, 1991*a*.

Dreger, D. S., and D. V. Helmberger, Complex faulting deduced from broadband modeling of the February 28, 1990 Upland earthquake (M_L = 5.2), *Bull. Seismol. Soc. Am., 81,* 1129-1144, 1991*b*.

Fan, G., and T. C. Wallace, The determination of source parameters for small earthquakes from a single very broadband seismic station, *Geophys. Res. Lett., 18,* 1385-1388, 1991.

Hadley, D., and K. Kanamori, Seismic structure of the Transverse Ranges, California, *Bull. Seismol. Soc. Am., 88,* 1469-1478, 1977.

Hadley, D., and K. Kanamori, Regional S-wave structure for southern California from the analysis of teleseismic Rayleigh waves, *Geophys. J. R. Astron. Soc., 58,* 655-666, 1979.

Helmberger, D. V., and G. R. Engen, Modeling the long-period body waves from shallow earthquakes at regional distances, *Bull. Seismol. Soc. Am., 70,* 1699-1714, 1980.

Helmberger, D. V., R. Stead, P. Ho-Liu and D. S. Dreger, Broadband modeling of regional seismograms; Imperial Valley to Pasadena, *Geophys. J. Int., 110,* 42-54, 1992*a*.

Helmberger, D. V., L. S. Zhao, D. S. Dreger and V. LeFevre, Exploration of the lower lithosphere; Northeastern United States, *Phys. Earth Planet. Inter., 70,* 22-38, 1992*b*.

Helmberger, D., D. Dreger, R. Stead, and H. Kanamori, Impact of broadband seismology on strong motion attenuation, *Bull. Seismol. Soc. Am.,* in press, 1993.

Ho-Liu, P., I. Attenuation tomography, II., Modeling regional love waves: Imperial Valley to Pasadena, Ph.D. thesis, Calif. Inst. of Technol., Pasadena, 1988.

Horton, S. P., and D. M. Depolo, The October 24, 1990 Lee Vining, California earthquake and other recent moderate earthquakes in the western Basin and Range, *Seismol. Res. Lett., 63,* 63, 1992.

Jones, L. M., and R. S. Dollar, Evidence of Basin-and-Range extensional tectonics in the Sierra Nevada: The Durwood Meadows Swarm, Tulare County, California (1983-1984), *Bull. Seismol. Soc. Am., 76,* 439-461, 1986.

Liu, H., and D. V. Helmberger, The 23:19 aftershock of the 15 October 1979 Imperial Valley earthquake: More evidence for an asperity, *Bull. Seismol. Soc. Am., 75,* 689-708, 1985.

Ma, K. F., and H. Kanamori, Aftershock sequence of the 3 December 1988 Pasadena earthquake, *Bull. Seismol. Soc. Am., 81,* 2310-2319, 1991.

Patton, H. J., and D. I. Doser, Inversion of regional P_{nl} and surface-wave data for the source parameters of the Borah Peak aftershock, *Geophys. Res. Lett., 15,* 459-462, 1988.

Shor, G. G., and E. Roberts, San Miguel, Baja California Norte, Earthquakes of February, 1956: A field report, *Bull. Seismol. Soc. Am., 48,* 101-116, 1958.

Stead, R. J., Finite differences and a coupled analytic technique with applications to explosions and earthquakes, Ph.D. thesis, Calif. Inst. of Technol., Pasadena, 1989.

Thio, H. K., and H. Kanamori, A surface wave study on the structure of the crust and upper mantle under southern California, *Eos Trans. AGU,* 72(44), Fall Meeting suppl., 324, 1991.

Wald, D. J., Strong motion and broadband teleseismic analysis of the 1991 Sierra Madre, California, earthquake, *J. Geophys. Res., 97,* 11033-11046, 1992.

Wallace, T. C., D. V. Helmberger, and G. R. Mellman, A technique for the inversion of regional data in source parameter studies, *J. Geophys. Res., 86,* 1679-1685, 1981.

Zhao, L. S., and D. V. Helmberger, Broadband modelling along a regional shield path, Harvard recording of the Saguenay earthquake, *Geophys. J. Int., 105,* 301-312, 1991.

D. S. Dreger, Seismographic Station, ESB 475, University of California, Berkeley, CA 94720.

D. V. Helmberger, Seismological Laboratory 252-21, California Institute of Technology, Pasadena, CA 91125.

(Received May 9, 1992;
revised December 21, 1992;
accepted December 29, 1992.)